Vertical sleeve gastrectomy confers metabolic improvements by reducing intestinal bile acids and lipid absorption in mice

Lili Ding[a,b], Eryun Zhang[a,b], Qiaoling Yang[a,c], Lihua Jin[b], Kyle M. Sousa[b,d], Bingning Dong[e], Yangmeng Wang[b], Jui Tu[b,f], Xiaoxiao Ma[b], Jingyan Tian[b], Hongli Zhang[b], Zhipeng Fang[b], Ana Guan[b], Yixin Zhang[a], Zhengtao Wang[a], David D. Moore[e,1,2], Li Yang[a,g,1], and Wendong Huang[b,f,1]

[a]Shanghai Key Laboratory of Complex Prescriptions and Ministry of Education Key Laboratory for Standardization of Chinese Medicines, Institute of Chinese Materia Medica, Shanghai University of Traditional Chinese Medicine, Shanghai 201203, China; [b]Department of Diabetes Complications and Metabolism, Diabetes and Metabolism Research Institute, Beckman Research Institute, City of Hope National Medical Center, Duarte, CA 91010; [c]Department of Pharmacy, Shanghai Children's Hospital, Shanghai Jiao Tong University, Shanghai 200062, China; [d]Department of Pharmaceutical and Administrative Sciences, School of Pharmacy, Loma Linda University, Loma Linda, CA 92350; [e]Department of Molecular and Cellular Biology, Baylor College of Medicine, Houston, TX 77030; [f]Graduate School of Biological Science, City of Hope National Medical Center, Duarte, CA 91010; and [g]Institute of Interdisciplinary Integrative Medicine Research, Shanghai University of Traditional Chinese Medicine, Shanghai 201203, China

Contributed by David D. Moore, December 8, 2020 (sent for review September 16, 2020; reviewed by Paul Dawson, Verena Keitel, and Antonio Moschetta)

Vertical sleeve gastrectomy (VSG) is one of the most effective and durable therapies for morbid obesity and its related complications. Although bile acids (BAs) have been implicated as downstream mediators of VSG, the specific mechanisms through which BA changes contribute to the metabolic effects of VSG remain poorly understood. Here, we confirm that high fat diet-fed global farnesoid X receptor (*Fxr*) knockout mice are resistant to the beneficial metabolic effects of VSG. However, the beneficial effects of VSG were retained in high fat diet-fed intestine- or liver-specific *Fxr* knockouts, and VSG did not result in Fxr activation in the liver or intestine of control mice. Instead, VSG decreased expression of positive hepatic Fxr target genes, including the bile salt export pump (*Bsep*) that delivers BAs to the biliary pathway. This reduced small intestine BA levels in mice, leading to lower intestinal fat absorption. These findings were verified in sterol 27-hydroxylase (*Cyp27a1*) knockout mice, which exhibited low intestinal BAs and fat absorption and did not show metabolic improvements following VSG. In addition, restoring small intestinal BA levels by dietary supplementation with taurocholic acid (TCA) partially blocked the beneficial effects of VSG. Altogether, these findings suggest that reductions in intestinal BAs and lipid absorption contribute to the metabolic benefits of VSG.

bile acids | bariatric surgery | farnesoid X receptor | cyp27a1 | lipid absorption

To date, bariatric surgery remains the most effective and long-lasting treatment for morbid obesity and its related complications, including type 2 diabetes (T2D) and fatty liver diseases (1, 2). The Roux-en-Y gastric bypass (RYGB) and vertical sleeve gastrectomy (VSG) surgical procedures represent two of the most commonly performed variations of bariatric surgery (3, 4). Because VSG results in fewer complications and a lower incidence of dumping syndrome, it thus has surpassed RYGB to become the most commonly performed bariatric procedure in the United States (4–6). Nevertheless, the precise relationship between the metabolic benefits of VSG and its underlying molecular mechanisms remains unclear.

Several molecular mechanisms associated with the metabolic benefits of bariatric surgery have been reported (7). While a number of studies have focused on the role of glucagon-like peptide 1 (GLP-1), whose circulating levels increase 5- to 10-fold after VSG (8, 9), glucagon-like peptide 1 receptor (GLP-1r) in β-cells appears dispensable for mediating improvements in glucose tolerance after surgery (10). Additional mechanisms underlying the benefits of VSG have been described and involve improved insulin secretion, substantial changes to islet gene expression (11), and alterations in the composition and concentration of bile acid (BA) digestive surfactants (12). For example, patients who receive bariatric surgery not only exhibit compositional changes to their pool of BAs but also experience an increase in their circulating concentrations (9, 13–15). In diet-induced obese rodent models, VSG recapitulates several of the observations perceived postsurgically in human patients, including significant changes in BA dynamics (16, 17). More interestingly, several studies have shown that the benefits of VSG may require two BA receptors: farnesoid X receptor (Fxr) and G protein-coupled BA receptor (also known as Tgr5) (18, 19). Although these observations underscore the potential importance of BA circulation and signaling in the metabolic benefits of bariatric surgery, the fundamental mechanisms through which BA changes confer such benefits remain unknown. Here, we analyze and compare

Significance

Vertical sleeve gastrectomy (VSG) is a highly effective bariatric surgery that sustainably treats obesity and type 2 diabetes (T2D). However, the underlying mechanisms governing its metabolic benefits remain unclear. In this study, we have used four different genetically modified mouse lines to understand the link between bile acid circulation and metabolic effects of VSG. Instead of directly activating the nuclear bile acid receptor farnesoid X receptor (Fxr) in the liver or intestine, VSG reduces intestinal levels of bile acids, thereby decreasing fat absorption in the intestine. Given the rising popularity of bariatric surgeries to treat obesity and associated T2D, the results described herein provide mechanistic insights that may lead to safer noninvasive approaches to mimic the metabolic effects of bariatric surgery.

Author contributions: D.D.M., L.Y., and W.H. designed research; L.D., E.Z., Q.Y., L.J., Y.W., and H.Z. performed research; B.D., J.Tu, X.M., J.Tian, Z.F., and A.G. contributed new reagents/analytic tools; L.D. and Y.Z. analyzed data; and L.D., K.M.S., Z.W., D.D.M., L.Y., and W.H. wrote the paper.

Reviewers: P.D., Emory University; V.K., Heinrich-HeineUniversität Düsseldorf; and A.M., University of Bari.

The authors declare no competing interest.

[1]To whom correspondence may be addressed. Email: moore@bcm.edu, yl7@shutcm.edu.cn, or whuang@coh.org.

[2]Present address: Department of Nutritional Science & Toxicology, University of California, Berkeley, CA 94720-3104.

This article contains supporting information online at https://www.pnas.org/lookup/suppl/doi:10.1073/pnas.2019388118/-/DCSupplemental.

Published February 1, 2021.

the effects of VSG in different mouse lines (*Fxr* whole-body knockout [$Fxr^{-/-}$], liver-specific knockout [$Fxr^{\Delta L}$], intestine-specific knockout [$Fxr^{\Delta IN}$], and *Cyp27a1* knockout [$Cyp27a1^{-/-}$]) and demonstrate that reduced intestinal BAs and lipid absorption may underlie the metabolic benefits of VSG.

Results

Hepatic or Intestinal Fxr Is Dispensable for the Metabolic Improvement of VSG. According to a previous report, the positive metabolic benefits of VSG are lost when *Fxr* is knocked out of mice (18). To better understand the role of Fxr in this process, we systematically

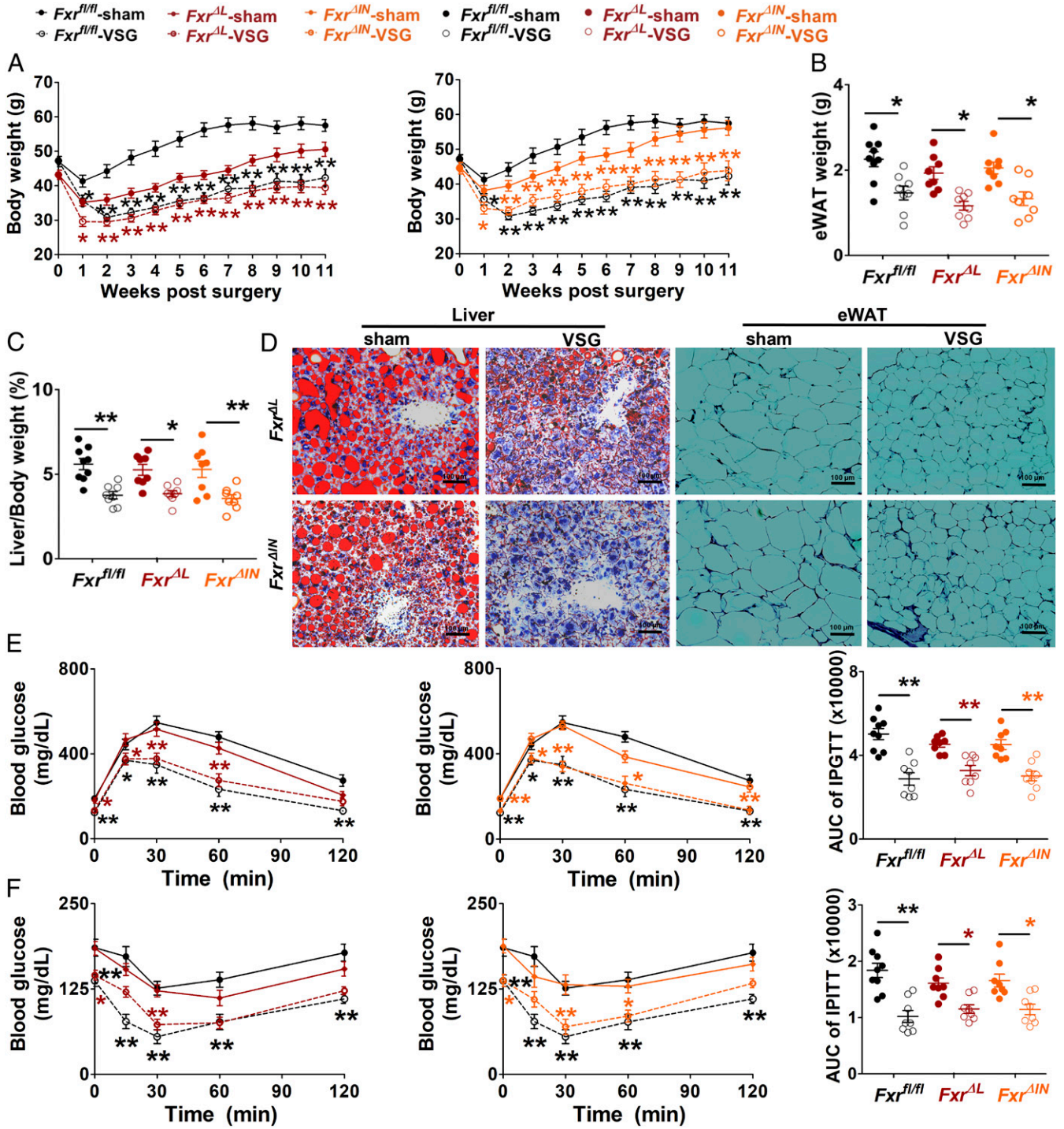

Fig. 1. The metabolic benefits of VSG are maintained in liver- and intestine-specific *Fxr* knockout mice. Liver-specific *Fxr* knockout ($Fxr^{\Delta L}$) mice and intestine-specific *Fxr* knockout ($Fxr^{\Delta IN}$) mice compared with $Fxr^{fl/fl}$ mice were fed with HFD for 10 wk and then subjected to VSG or sham surgery ($n = 8$ to 9). (*A*) Body weight of $Fxr^{fl/fl}$, $Fxr^{\Delta L}$, and $Fxr^{\Delta IN}$ mice during 11 wk postsurgery. (*B*) Weight of eWAT and (*C*) the liver-to-body weight ratio of mice at 12 wk postsurgery. (*D*) The representative images of Oil red O staining of liver sections and hemotoxylin and eosin staining of eWAT sections. (*E*) Intraperitoneal glucose tolerance test (IPGTT) and the areas under curve (AUCs) at 11 wk postsurgery. (*F*) Intraperitoneal insulin tolerance test (IPITT) assay and the AUC at 12 wk postsurgery. Values are mean ± SEM. $^*P < 0.05$, $^{**}P < 0.01$ by one-way ANOVA and Tukey's post hoc test.

assessed the impact of VSG in several mouse models. First, a group of *Fxr* floxed/floxed control mice ($Fxr^{fl/fl}$) were compared with an independently generated, whole-body *Fxr* knockout ($Fxr^{-/-}$) mouse line as we have previously described (20). Significant improvements were noted in phenotypes related to obesity, diabetes, and fatty liver disease following VSG in $Fxr^{fl/fl}$ mice (*SI Appendix*, Fig. S1). Conversely, VSG failed to improve these metabolic phenotypes in $Fxr^{-/-}$ mice (*SI Appendix*, Fig. S1). We next assessed the tissue-specific impacts of Fxr. Previous reports indicate that regulation of lipid metabolism, glucose metabolism, and other physiological functions may require modulation of Fxr in either the liver or intestine (21–23). Therefore, we performed VSG (following high-fat diet [HFD] feeding) on either liver-specific knockout mice ($Fxr^{\Delta L}$) or intestine-specific knockout mice ($Fxr^{\Delta IN}$). In the first 3 wk postsurgery, the food intake was significantly decreased in both *Fxr* conditional knockout mice after VSG when compared with sham surgery mice (*SI Appendix*, Fig. S2*A*). However, when the changes in food intake had ceased to exist by week 4, both $Fxr^{\Delta L}$ and $Fxr^{\Delta IN}$ mice still maintained the beneficial metabolic effects of VSG (Fig. 1) compared with sham-operated mice. Decreases were observed in body weight gain (Fig. 1*A*), weight of epididymal white adipose tissue (eWAT) (Fig. 1*B*), inguinal white adipose tissue (iWAT) (*SI Appendix*, Fig. S2*C*), liver weight, and liver-to-body weight ratio (Fig. 1*C* and *SI Appendix*, Fig. S2*B*). Five additional benefits of VSG were also observed in $Fxr^{\Delta L}$ and $Fxr^{\Delta IN}$ mice, including improved hepatosteatosis (Fig. 1*D* and *SI Appendix*, Fig. S2*D*), reduced adipocyte hypertrophy (Fig. 1*D* and *SI Appendix*, Fig. S2*D*), improved glucose tolerance, improved insulin

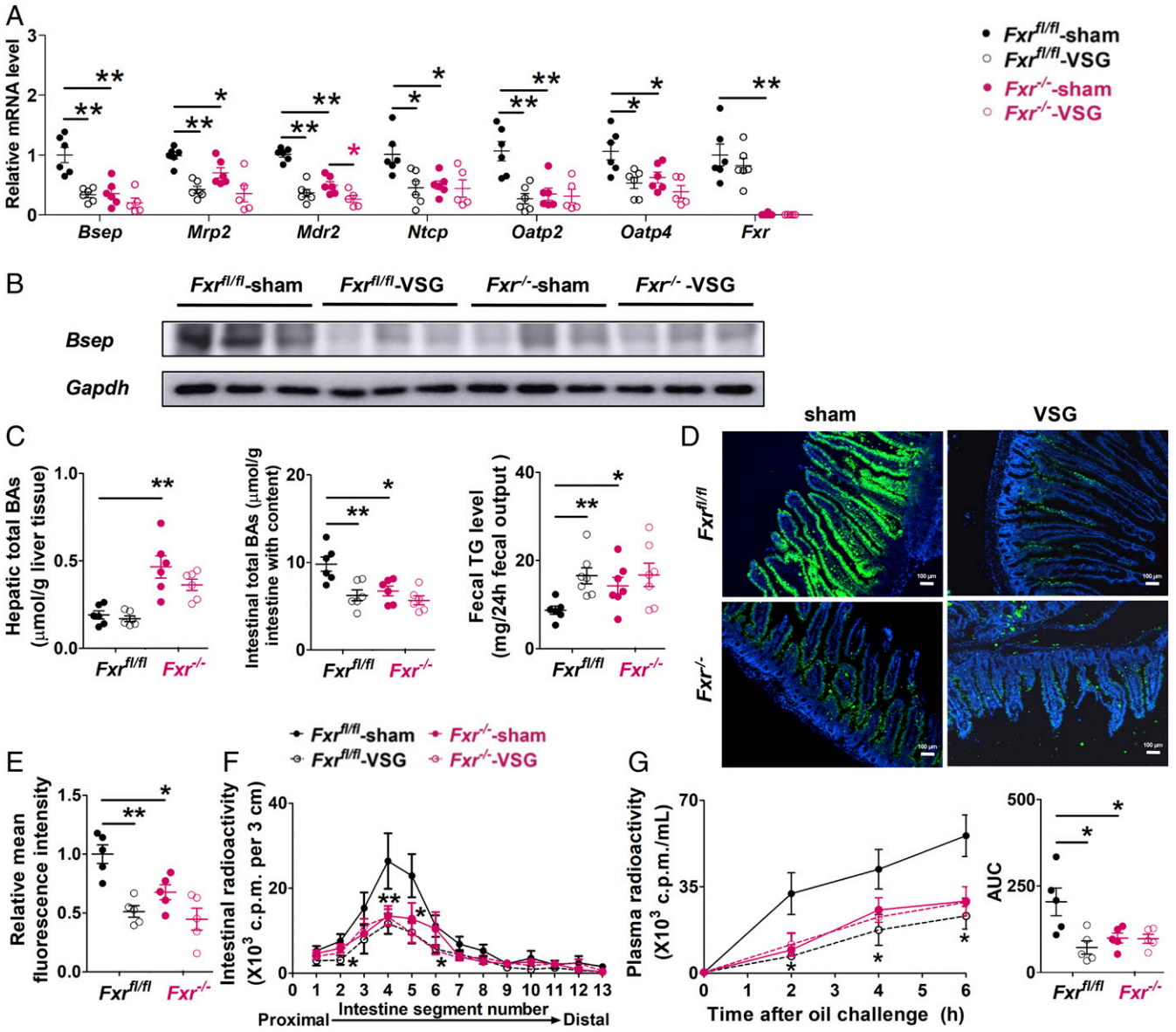

Fig. 2. VSG or *Fxr* deficiency reduces intestinal BA levels and fat absorption. $Fxr^{fl/fl}$ and $Fxr^{-/-}$ mice were fed with HFD for 10 wk and then subjected to VSG or sham surgical procedures for 4 wk. (*A*) Relative mRNA expression of genes ($n = 6$) and (*B*) western blotting analysis of Bsep in the liver tissues of mice. (*C*) Hepatic and intestinal total BAs levels and fecal triglycerides (TGs) levels of mice ($n = 6$ to 7). (*D*) Representative images of BODIPY staining of the proximal jejunum sections of mice. Scale bars: 100 μM. (*E*) The relative mean fluorescence intensity was determined by the average of three representative images from each mouse ($n = 5$). (*F*) The levels of radioactivity of ^{14}C-triolein at 2 h after olive oil containing ^{14}C-triolein administration in intestinal segments of mice were recorded by the value of counts per minute (c.p.m.) ($n = 5$). (*G*) The levels of plasma radioactivity in mice subjected to surgery for 4 wk. The areas under the curve (AUCs) are shown ($n = 5$). Values are mean ± SEM. $^*P < 0.05$, $^{**}P < 0.01$ by one-way ANOVA and Tukey's post hoc test.

sensitivity, and lower levels of fasting blood glucose and insulin (Fig. 1 *E* and *F* and *SI Appendix*, Fig. S2 *E* and *F*). Thus, neither liver nor intestine knockout of *Fxr* were sufficient to abolish the beneficial effects of VSG.

To investigate whether VSG may require the activation of both intestine and liver Fxr to confer its metabolic improvements, we analyzed the messenger RNA (mRNA) expression levels of the FXR transcriptional target genes. As expected, mRNA levels of positive hepatic and intestinal Fxr target genes (Fig. 2*A* and *SI Appendix*, Fig. S3*A*) were significantly decreased in $Fxr^{-/-}$-sham mice compared with $Fxr^{fl/fl}$-sham mice. The expression of hepatic Fxr target genes, including *bile salt-export pump* (*Bsep*), *multidrug resistance-associated protein 2* (*Mrp2*), *multidrug resistance protein 2* (*Mdr2*), *sodium-taurocholate cotransporting polypeptide* (*Ntcp*), *organic solute transporter 2* (*Oatp2*), *organic solute transporter 4* (*Oatp4*), and the intestinal Fxr target gene *ileal BA-binding protein* (*Ibabp*), was significantly suppressed after VSG compared with sham-operated $Fxr^{fl/fl}$ mice (Fig. 2*A* and *SI Appendix*, Fig. S3*A*). The hepatic BA transporter Bsep is a key mediator of the transport of BAs from the liver to the gallbladder for subsequent release into the small intestine to promote lipid absorption (24), and Bsep protein levels are dramatically decreased in human patients with loss of Fxr function (25). We confirmed that hepatic Bsep protein was decreased not only in $Fxr^{-/-}$-sham mice relative to $Fxr^{fl/fl}$-sham but also in $Fxr^{fl/fl}$-VSG mice, which was consistent with decrease in Bsep transcripts (Fig. 2*B*). It should be noted that the expression levels of *Fxr* in both liver and intestine tissues were sustained in $Fxr^{fl/fl}$ mice after VSG (Fig. 2*A* and *SI Appendix*, Fig. S3*A*).

Decreased Intestinal BA Levels and Lipid Absorption in the Small Intestine after VSG. Interestingly, we observed that $Fxr^{-/-}$ mice and VSG-operated $Fxr^{fl/fl}$ mice shared some similar phenotype (*SI Appendix*, Fig. S1) in the context of decreased expression of Bsep (Fig. 2*B*). Furthermore, some similar gene expression profiles were observed between $Fxr^{-/-}$ mice and VSG-operated $Fxr^{fl/fl}$ mice (Fig. 2*A* and *SI Appendix*, Fig. S3*A*), suggesting that VSG may confer BA alterations similar to those associated with *Fxr* knockout. It has been shown that deletion of *Fxr* results in cholestasis due to a failure in the maintenance of the enterohepatic BA circulation (26, 27). Because a primary function of BAs is to emulsify lipids and facilitate the absorption of lipids in the small intestine, we next asked whether the altered BA circulation by VSG leads to reduced BA levels and decreased fat absorption in small intestine.

To address this, we first measured the total BA levels in the small intestine of VSG- or sham-operated mice at an early stage postsurgery. Hepatic total BAs levels were not altered in both $Fxr^{fl/fl}$ and $Fxr^{-/-}$ mice after VSG (*SI Appendix*, Fig. S2*G*), but BA levels in the small intestines of $Fxr^{-/-}$-sham mice and the VSG-operated $Fxr^{fl/fl}$ mice were significantly lowered compared with $Fxr^{fl/fl}$-sham mice (Fig. 2*C*). Consequently, the levels of excreted fecal lipids were significantly higher in $Fxr^{-/-}$-sham and $Fxr^{fl/fl}$-VSG mice than in $Fxr^{fl/fl}$-sham mice (Fig. 2*C*). To test if VSG may reduce intestinal lipid absorption, we gavaged mice with ^{14}C-labeled trioleoylglycerol and measured radioactivity incorporation along the length of the small intestine to measure the uptake of dietary fat. As expected, histological examination of proximal jejunum sections stained with 4,4-difluoro-4-bora-3a,4a-diaza-s-indacene (BODIPY) from mice gavaged with olive oil showed a strong reduction in lipid droplet accumulation in $Fxr^{-/-}$-sham and $Fxr^{fl/fl}$-VSG mice (Fig. 2 *D* and *E*). Moreover, decreased fat absorption was observed in the proximal jejunum of $Fxr^{-/-}$-sham and $Fxr^{fl/fl}$-VSG mice compared with $Fxr^{fl/fl}$-sham mice (Fig. 2*F*). Next, we assessed the rate of triacylglycerol entry into plasma in mice gavaged with radiolabeled trioleoylglycerol. Mice were injected in advance with tyloxapol to inhibit plasma lipolysis (28). Radioactivity abundance in plasma accumulated more slowly in $Fxr^{-/-}$-sham and $Fxr^{fl/fl}$-VSG mice vs. $Fxr^{fl/fl}$-sham mice (Fig. 2*G*), indicating reduced entry of lipid into the systemic circulation. These results demonstrate that *Fxr* knockout and VSG surgery both result in reduced fat absorption.

The expression profile of genes involved in the transport of BAs may explain the underlying mechanism driving decreased intestinal BAs in $Fxr^{-/-}$ and $Fxr^{fl/fl}$-VSG mice (Fig. 2*A* and *SI Appendix*, Fig. S3*A*). Although the profile of BA synthetic genes differed between $Fxr^{-/-}$ mice and VSG-operated $Fxr^{fl/fl}$ mice (*SI Appendix*, Fig. S3*B*), similar profiles in BA transport genes were observed (Fig. 2*A* and *SI Appendix*, Fig. S3*A*). More specifically, the expression of hepatic genes involved in BA transport to the intestine (*Bsep*, *Mrp2*, and *Mdr2*) was significantly decreased in $Fxr^{fl/fl}$-VSG mice, as well as in $Fxr^{-/-}$ mice (Fig. 2 *A* and *B*). However, the expression of *apical sodium–BA transporter* (*Asbt*), a transporter that regulates uptake of BAs into the ileum, remained unchanged (*SI Appendix*, Fig. S3*A*), thus explaining the decreased BA level in the intestine. The increased levels of circulating plasma BAs in $Fxr^{fl/fl}$-VSG mice are likely explained by the increased expression of *multidrug resistance-associated protein* (*Mrp3*), a transporter that mediates the secretion of BAs into the circulation (*SI Appendix*, Fig. S3*B*), and decreased levels of *Ntcp*, *Oatp2* and *Oatp4* (in both $Fxr^{-/-}$-sham and $Fxr^{fl/fl}$-VSG mice), which are transporters responsible for the hepatic uptake of BAs from the circulation (Fig. 2*A*).

Compared with the sham-operated $Fxr^{fl/fl}$ mice, both the VSG-operated $Fxr^{fl/fl}$ mice and the whole-body *Fxr* knockout mice had dramatically reduced small intestinal levels of taurine-conjugated BAs (*SI Appendix*, Fig. S4*A*). In addition to taurocholic acid (TCA), cholic acid (CA) and glycocholic acid (GCA) were dramatically decreased in $Fxr^{-/-}$ and VSG-$Fxr^{fl/fl}$ mice (*SI Appendix*, Fig. S4). Interestingly, CA, TCA, and GCA all represent 12α-hydroxylated BAs. It has been reported that CA plays an important role in promoting intestinal cholesterol absorption (29) and that 12α-hydroxylated BAs are associated with insulin resistance and high triglyceride levels (30). Our results suggest that specific changes in 12α-hydroxylated BAs may also contribute to the metabolic improvements after VSG.

The Decrease in Intestinal BA Levels following VSG Is Independent of Hepatic or Intestinal FXR. To confirm the relationship between BA levels in small intestine and the metabolic effect of VSG, we then measured the total BA levels of small intestine and compositions in each surgical cohort at week 4 postsurgery. Similar to $Fxr^{fl/fl}$ mice, $Fxr^{\Delta L}$ and $Fxr^{\Delta IN}$ mice showed markedly decreased small intestinal BA levels following VSG (Fig. 3*A*), accompanied with increased fecal triglycerides excretion (Fig. 3*B*). Meanwhile, more droplets were evident in the proximal jejunum of tissue-specific *Fxr* knockout mice at 2 h after oral oil administration (Fig. 3 *C* and *D*). Similar results with lipid absorption were also observed in tissue-specific knockout mice (Fig. 3 *E* and *F*), further suggesting that instead of activating Fxr in liver or intestine, a reduced BA level in the small intestine may contribute to the reduced intestinal lipid absorption after VSG.

BA composition in the small intestine showed that the levels of most taurine-conjugated BAs were significantly decreased in $Fxr^{\Delta IN}$ and $Fxr^{\Delta L}$ mice following VSG (*SI Appendix*, Fig. S5). In particular, $Fxr^{\Delta IN}$ or $Fxr^{\Delta L}$ deficiency reduced TCA levels by 66 and 56%, respectively, after VSG (*SI Appendix*, Fig. S5), this decrease may profoundly affect lipid absorption (Fig. 3 *B*–*F*).

BA profiles have direct impact on gut microbiota. We thus analyzed the gut microbiota in these cohorts of mice (*SI Appendix*, Fig. S6). At the phylum level, VSG significantly decreased the Firmicutes-to-Bacteroidetes ratio in $Fxr^{fl/fl}$, $Fxr^{\Delta L}$, and $Fxr^{\Delta IN}$ mice, but not in $Fxr^{-/-}$ mice (*SI Appendix*, Fig. S6 *A* and *B*). Bile salt hydrolase (BSH) deconjugates taurine-conjugated BAs to free BAs through the hydrolysis of the C24 *N*-acyl amide bond of conjugated BAs (31). At the genus level, *Lactobacillus*, which carries BSH enzymes, was significantly increased in $Fxr^{fl/fl}$, $Fxr^{\Delta L}$, and $Fxr^{\Delta IN}$ mice post-VSG, but not in $Fxr^{-/-}$ mice (*SI Appendix*, Fig. S6*C*).

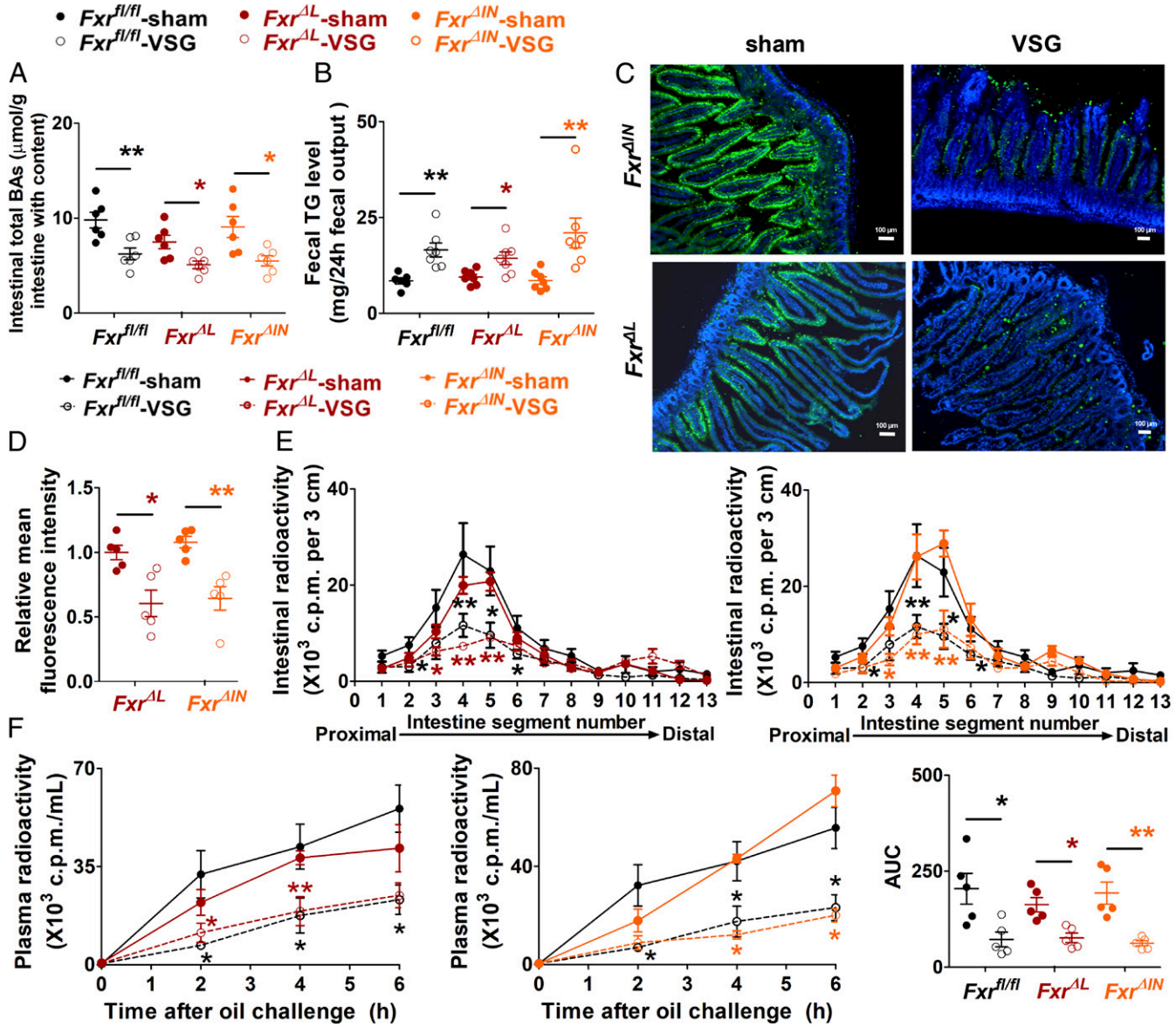

Fig. 3. The decrease of intestinal BA levels and lipid absorption after VSG is independent of hepatic or intestinal Fxr. $Fxr^{\Delta L}$ mice and $Fxr^{\Delta IN}$ mice compared with $Fxr^{fl/fl}$ mice were fed with HFD for 10 wk and then subjected to VSG or sham surgical procedures for 4 wk. (*A*) Intestinal total BAs levels and (*B*) fecal triglycerides (TGs) levels of mice ($n = 6$ to 7). (*C*) Representative images of BODIPY staining of the proximal jejunum sections of mice. Scale bars: 100 μM. (*D*) The relative mean fluorescence intensity was determined by the average of three representative images from each mouse ($n = 5$). (*E*) The levels of radioactivity of ^{14}C-triolein at 2 h after olive oil containing ^{14}C-triolein administration in intestinal segments of mice were recorded by the value of counts per minute (c.p.m.) ($n = 5$). (*F*) The levels of plasma radioactivity in mice subjected to surgery for 4 wk and the areas under the curve (AUCs; $n = 5$). Values are mean ± SEM. $^*P < 0.05$, $^{**}P < 0.01$ by one-way ANOVA and Tukey's post hoc test.

In addition, we observed that the members of the genus *Bacteroides*, which express BA 7-α-hydroxysteroid dehydrogenases (32), were significantly increased in $Fxr^{fl/fl}$, $Fxr^{\Delta L}$, and $Fxr^{\Delta IN}$ mice, but not in $Fxr^{-/-}$ mice following VSG (*SI Appendix*, Fig. S6*D*). Overall, although tissue-specific Fxr knockout mice exhibited a different profile in BA synthetic enzymes and transporters (*SI Appendix*, Fig. S7), our data suggest that VSG markedly altered BA synthesis and circulation, as well as the gut microbiota, which may contribute to reduced intestinal lipid absorption.

***Cyp27a1*$^{-/-}$ Mice Show Reduced Fat Absorption and Lose the Metabolic Effects following VSG.** We sought out to further probe the relationship between VSG and BA-regulated absorption of intestinal lipids. To this end, we turned to a mouse model lacking the enzyme sterol 27-hydroxylase (Cyp27a1); this mouse model harbors low levels of intestinal BAs. *Cyp27a1*$^{-/-}$ mice both disturbed synthesis pathway and transport pathway (*SI Appendix*, Fig. S8 *A* and *B*) and displayed a dramatic reduction of 73% in the BA pool and a decrease of 79% total BAs in the small bowel (33, 34) compared with wild-type (Wt) mice. Importantly, compared with Wt mice, *Cyp27a1*$^{-/-}$ mice have a 2.5-fold increase in fecal sterol excretion (34). When placed on an HFD, *Cyp27a1*$^{-/-}$ mice were resistant to weight gain (*SI Appendix*, Fig. S9 *A* and *B*). After 10 wk on an HFD, the fasting blood glucose level and glucose tolerance test (GTT) of *Cyp27a1*$^{-/-}$ mice were significantly improved when compared with Wt mice (*SI Appendix*, Fig. S9 *C* and *D*). Additionally, after being fed with HFD, *Cyp27a1*$^{-/-}$ and Wt mice were injected with tyloxapol and then orally gavaged with olive oil for testing the plasma triglyceride levels. Plasma

triglyceride levels were significantly lower in the *Cyp27a1*$^{-/-}$ mice (*SI Appendix*, Fig. S9*E*). Collectively, these results suggest *Cyp27a1*$^{-/-}$ mice exhibit decreased intestinal lipid absorption.

We further probed the effects of VSG on the small intestinal BA levels and lipid absorption. Both the hepatic and small intestinal BA levels in *Cyp27a1*$^{-/-}$-sham mice were significantly lower (30 and 44% of Wt-sham mice, respectively) (Fig. 4*A*), but the concentration of excreted fecal triglycerides was significantly higher than that of Wt-sham mice (Fig. 4*A*). Importantly, no differences in these indicators were observed between the sham- or VSG-operated *Cyp27a1*$^{-/-}$ mice (Fig. 4*A*). These results were confirmed in experiments using radiolabeled trioleoylglycerol. Histological examination of proximal jejunum sections stained with BODIPY showed reductions in lipid droplet accumulation in *Cyp27a1*$^{-/-}$-sham and Wt-VSG mice (Fig. 4 *B* and *C*). Consistently, the decreased radioactivity was observed along the proximal small intestine (Fig. 4*D*) and less radioactivity in plasma of *Cyp27a1*$^{-/-}$-sham and Wt-VSG mice (Fig. 4*E*). Levels of CA, TCA, and GCA in the small intestine were all significantly lower in *Cyp27a1*$^{-/-}$-sham and Wt-VSG mice relative to Wt-sham mice (*SI Appendix*, Fig. S8*C*). We hypothesized that the aforementioned effects of VSG on Wt mice could not be extended further in *Cyp27a1*$^{-/-}$ mice, as we observed in *Fxr*$^{-/-}$ mice. To test this, Wt and *Cyp27a1*$^{-/-}$ mice were fed an HFD for several weeks prior to performing VSG or sham surgical procedures. The surgery produced significant differences of food intake at the first 2 to 3 wk in Wt and *Cyp27a1*$^{-/-}$ mice (*SI Appendix*, Fig. S10*A*). However, by the fourth week following VSG, when the discrepancy of food intake was abolished, VSG still failed to induce any further weight loss in *Cyp27a1*$^{-/-}$ mice (Fig. 4*F*). At 12 wk postsurgery, we assessed the liver-to-body weight ratio, the eWAT, and iWAT weight (*SI Appendix*, Fig. S10*B*) of these mice. We also performed a histological analysis of fatty liver and adipocyte hypertrophy (Fig. 4*G* and *SI Appendix*, Fig. S10*C*). In general, the values of these parameters were similar for the *Cyp27a1*$^{-/-}$-sham mice and Wt-VSG mice. Additionally, the parameters for both *Cyp27a1*$^{-/-}$-sham mice and Wt-VSG mice were significantly lower than those of the Wt-sham mice. VSG failed to further improve several metabolic phenotypes in *Cyp27a1*$^{-/-}$ mice (Fig. 4*G* and *SI Appendix*, Fig. S10*C*). Similar results were observed for glucose tolerance, insulin sensitivity, fasting blood glucose, and insulin levels (Fig. 4 *H* and *I* and *SI Appendix*, Fig. S10*D*).

Oral TCA Supplementation Partially Reverses VSG-Induced Metabolic Improvements. Because TCA levels were dramatically decreased in the small intestine and accompanied with reduced fat absorption in *Fxr*$^{fl/fl}$ mice after VSG, we asked whether TCA supplementation could reverse the metabolic improvements conferred by VSG. Both *Fxr*$^{fl/fl}$-sham and *Fxr*$^{fl/fl}$-VSG mice were orally administered TCA for 6 wk after VSG. As expected, TCA administration diminished the metabolic benefits of VSG (Fig. 5 *A*–*C* and *SI Appendix*, Fig. S11). At the fifth and sixth weeks after surgery, the body weight of *Fxr*$^{fl/fl}$-VSG mice with TCA treatment rebounded to a level comparable with *Fxr*$^{fl/fl}$-sham mice treated with TCA and showed significant differences compared with *Fxr*$^{fl/fl}$-VSG mice treated with vehicle control (Fig. 5*A*). Food consumptions were similar by week 4 postsurgery (Fig. 5*B*). Meanwhile, the GTT, liver-to-body weight ratios, and iWAT weight of *Fxr*$^{fl/fl}$-VSG mice with TCA administration displayed significant discrepancy compared with the *Fxr*$^{fl/fl}$ surgical cohorts without TCA treatment (Fig. 5*C* and *SI Appendix*, Fig. S11), whereas the food intake was still comparable with *Fxr*$^{fl/fl}$-VSG mice (Fig. 5*B*). As expected, the lowered BAs pool of small intestine and induced excretion of fecal triglycerides by VSG were impaired by the treatment of TCA in *Fxr*$^{fl/fl}$ mice (Fig. 5 *D* and *E*). Meanwhile, the level of hepatic BAs was also significantly elevated (Fig. 5*D*). Remarkably, the significant difference of radioactivity abundance in plasma of *Fxr*$^{fl/fl}$-sham and *Fxr*$^{fl/fl}$-VSG mice was lost after TCA treatment (Fig. 5*F*). Taken together, these results suggest that oral administration of TCA restores the intestinal BAs and consequently, partially reverses the metabolic effects conferred by VSG.

Discussion

To date, bariatric surgery remains the only viable therapeutic option for sustainable weight loss, T2D remission, and improvements in hepatosteatosis (1, 2, 35). However, the molecular mechanisms underpinning the beneficial effects of surgery remain uncertain. Surgical studies performed with transgenic mice seem uniquely positioned to address this, but the results of such studies have not yielded a clear consensus mechanism. Among the molecular pathways interrogated thus far, BAs and BA signaling appear to be indispensable players in mediating the metabolic improvements associated with bariatric surgery. In this study, we show that VSG triggers a decrease in intestinal BA content that decreases fat absorption. This dynamic in the enterohepatic circulation of BAs contributes to the profound impact of VSG on systemic metabolism in concert with other pathways. Indeed, we previously showed that VSG increased levels of BAs in the blood circulation and activated the membrane BA receptor Tgr5, concomitant with improved glucose control and increased energy expenditure (19). Thus, Tgr5 may be a molecular target and mediator of VSG. An earlier study showed that *Fxr* knockout mice almost completely lose the major beneficial effects of VSG on body weight loss and glucose lowering (18), and our current results with a distinct *Fxr* knockout strain are concordant. As a primary BA receptor, Fxr regulates BA enterohepatic circulation in both the liver and intestine by transcriptionally regulating BA synthesis, transporters, and other related genes. Thus, this genetic result suggests a role for Fxr activation in response to VSG, and we were surprised that we did not find evidence for such activation in liver or intestine. Instead, we observed either suppression or no changes in positive Fxr target genes in both the liver and ileum in response to VSG, notably including *Bsep*. Future investigation will be needed to address the mechanism by which VSG affects these BA gene targets. However, our results suggest that VSG may not work through Fxr activation and that *Fxr* knockout and VSG may confer metabolic improvements by an alternative pathway(s). Although Fxr agonists have been generally known to impart metabolic benefits (36–38), several previous reports have shown that Fxr antagonism can also generate beneficial metabolic effects (39–42). This apparent paradox suggests the existence of either distinct or partially overlapping mechanisms by which both gain and loss of Fxr function can generate metabolic improvement. Such pathways could explain why the beneficial effects of increasing BA levels by surgical bile diversion to the ileum are dependent on intestinal Fxr (43).

BA circulation is an evolutionally conserved mechanism that is essential for nutrient absorption and other systemic metabolic processes. The primary physiological function of BAs is to facilitate the intestinal absorption of dietary fats and fat-soluble vitamins (29, 44, 45). In the present study, we explore the factors that drive the decrease in intestinal BA content of obese mice subjected to VSG. On one hand, our results showed that mRNA as well as protein levels of Besp significantly decreased, reducing the intestinal BAs pool size and in accord with other studies of the impact of decreased Bsep expression (25), significantly influencing intestinal fat absorption. On the other hand, an increase in gut permeability induced by VSG or loss of Fxr activity might also contribute to reduced intestinal BA content by promoting paracellular uptake of BAs in the proximal gut. Blanchard et al. (46) exhibited that the distal colon paracellular and transcellular permeability of obese mice tended to be increased at the fourth week post-sleeve gastrectomy. Additionally, mice lacking Fxr experienced bacterial overgrowth and increased intestinal permeability (47). These earlier reports and our current

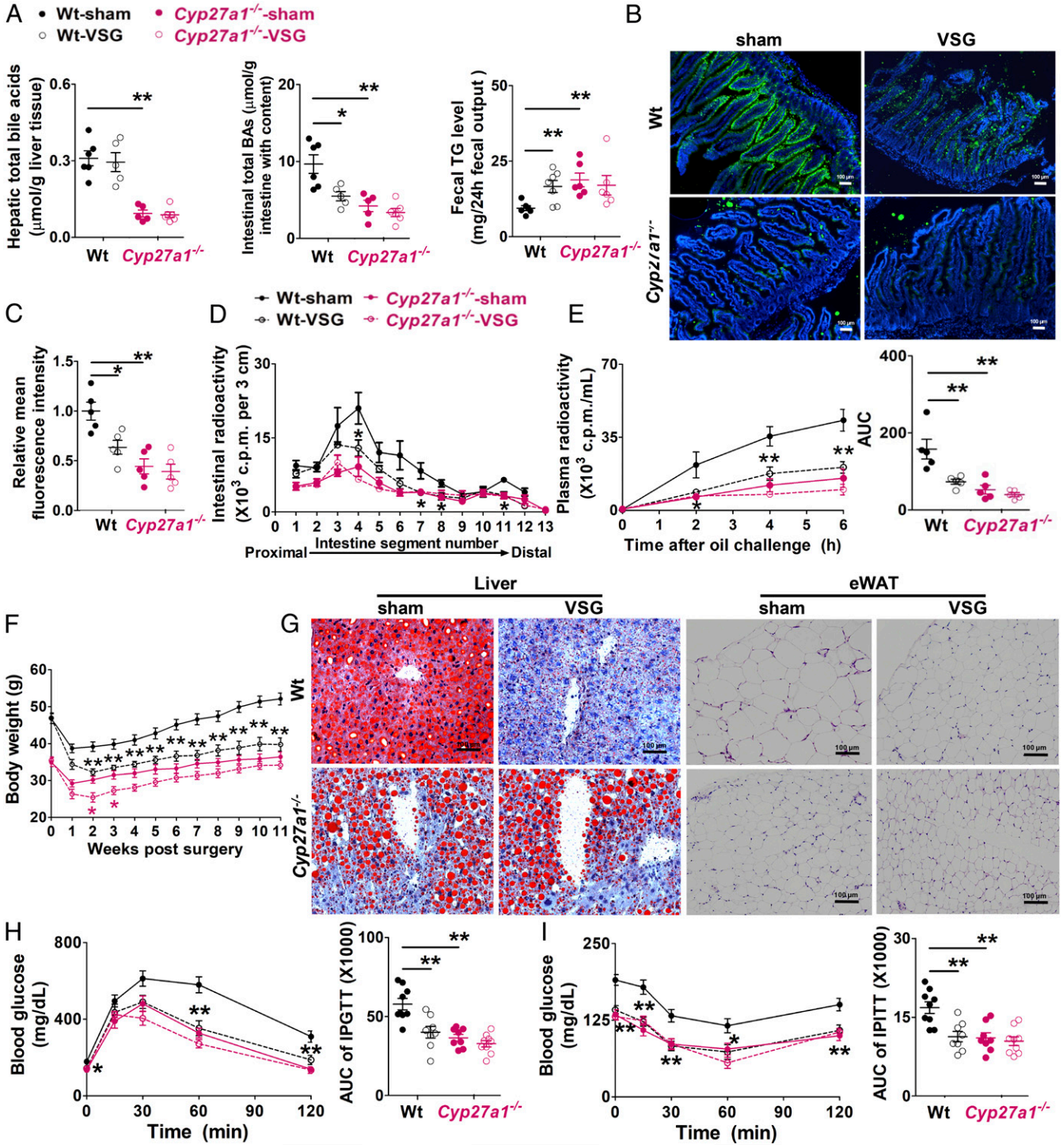

Fig. 4. *Cyp27a1*$^{-/-}$ mice display lower intestinal BA levels and decreased fat absorption following VSG; Wt and *Cyp27a1*$^{-/-}$ mice were fed HFD for 10 wk and then subjected to VSG or sham surgical procedures for 4 wk (*A*–*E*) or 12 wk (*F*–*I*). (*A*) Hepatic and intestinal total BAs levels and fecal triglycerides (TGs) levels of mice (n = 5 to 7). (*B*) Representative images of BODIPY staining of the proximal jejunum sections of mice. Scale bars: 100 μM. (*C*) The relative mean fluorescence intensity was determined by the average of three representative images from each mouse (n = 5). (*D*) The levels of radioactivity of ^{14}C-triolein at 2 h after olive oil containing ^{14}C-triolein administration in intestinal segments of mice were recorded by the value of counts per minute (c.p.m.) (n = 5). (*E*) The levels of plasma radioactivity in mice subjected to surgery for 4 wk and the areas under the curve (AUCs; n = 5). (*F*) Body weight of mice during 11 wk postsurgery. (*G*) Representative images of the Oil red O staining of liver sections and hemotoxylin and eosin staining of eWAT of mice at 12 wk postsurgery. Scale bars: 100 μM. (*H*) Intraperitoneal glucose tolerance test (IPGTT) and its corresponding AUC measured at 11 wk postsurgery. (*I*) Intraperitoneal insulin tolerance test (IPITT), its corresponding AUC, and the fasting blood insulin levels of mice measured at 12 wk postsurgery. Values are mean ± SEM. *P < 0.05, **P < 0.01 by one-way ANOVA and Tukey's post hoc test.

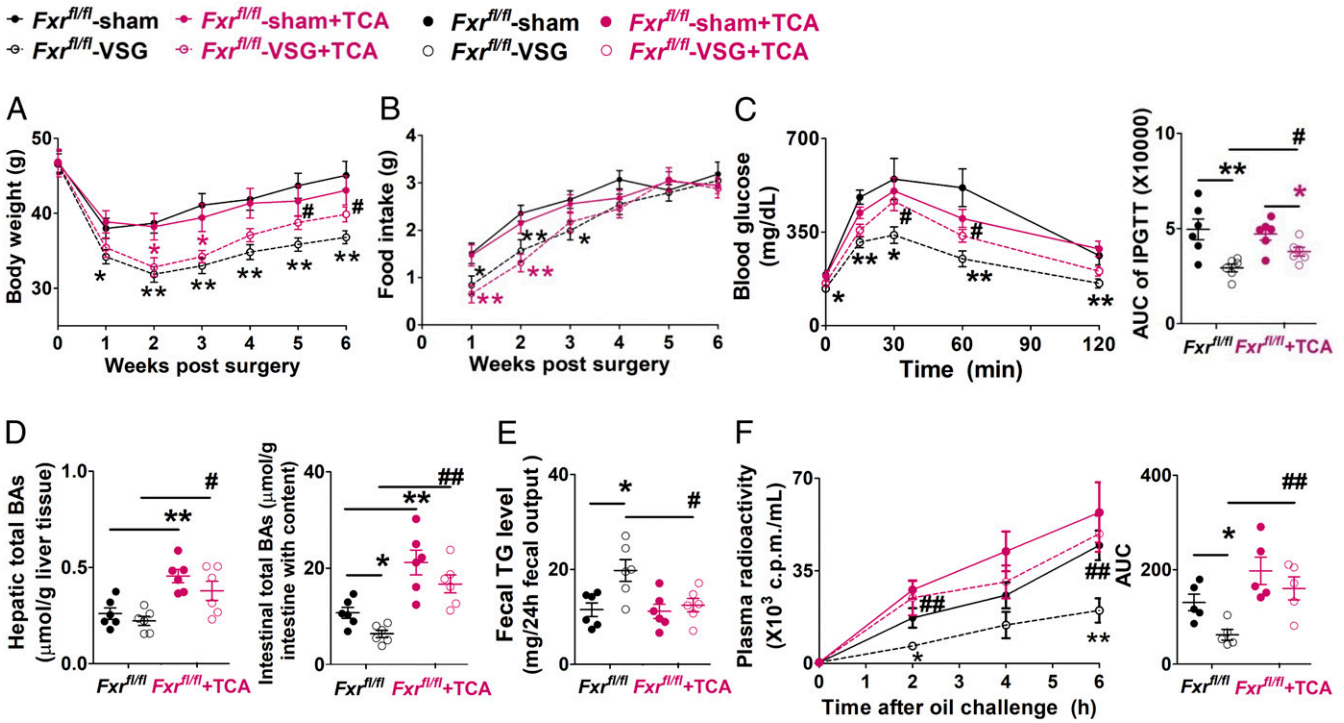

Fig. 5. Dietary supplementation with TCA reverses VSG-induced metabolic improvements. *Fxr*$^{fl/fl}$ mice were fed HFD and then subjected to VSG or sham surgical procedures. After being fed diet gel for 3 d, *Fxr*$^{fl/fl}$-VSG mice were reintroduced to HFD mixed with TCA for 6 wk. (*A*) Body weight and (*B*) food intake of mice during 6 wk postsurgery ($n = 6$). (*C*) Intraperitoneal glucose tolerance test (IPGTT) and the corresponding areas under curve (AUCs) measured at 6 wk postsurgery ($n = 6$). (*D*) Hepatic and small intestinal total BAs levels and (*E*) fecal triglycerides (TGs) levels of mice ($n = 6$). (*F*) The levels of plasma radioactivity were recorded by the value of counts per minute (c.p.m.) in mice subjected to surgery for 6 wk and the AUC ($n = 5$). Values are mean ± SEM. $^{*}P < 0.05$, $^{**}P < 0.01$ vs. *Fxr*$^{fl/fl}$-sham mice or *Fxr*$^{fl/fl}$-sham mice treated with TCA; $^{\#}P < 0.05$, $^{\#\#}P < 0.01$ vs. *Fxr*$^{fl/fl}$-VSG mice by one-way ANOVA and Tukey's post hoc test.

data suggest that this mechanism for decreased caloric intake, or possibly decreased Fxr signaling, could contribute to the metabolic improvements conferred by VSG.

We confirmed similar observations in *Cyp27a1*-deficient mice, which have a lower enterohepatic BA pool (33). Our analyses revealed that *Cyp27a1* knockout mice have reduced BA levels in the small intestine and decreased intestinal fat absorption in a manner similar to that observed following VSG. As expected, *Cyp27a1*-deficient mice lost the metabolic benefits of VSG. By analyzing and comparing the effects of bariatric surgery in four independent genetic mouse models (*Fxr*$^{-/-}$, *Fxr*$^{\Delta L}$, *Fxr*$^{\Delta IN}$, and *Cyp27a1*$^{-/-}$), our results suggest that reduced BA levels in the small intestine and decreased lipid absorption could contribute to beneficial metabolic changes conferred by VSG. Although we are not aware of any direct assessment of the impact of VSG on luminal small intestine BAs in humans, our results are consistent with the clear metabolic benefits of the BA sequestrant cholesevalam in both rodents and humans (48–50).

VSG generates significant changes of production, secretion, and redistribution of BAs. In our previous study, we identified that Tgr5 is activated by the increased BA levels in the blood circulation after VSG. In this study, we confirm previous observations and further show that VSG decreases BA levels in the intestine, which leads to impaired intestinal lipid absorption. Therefore, VSG leads to a dynamic of the enterohepatic circulation of BAs, which profoundly impacts the systemic metabolism. The anatomical changes in RYGB and VSG are very different. Intestinal anatomy is intact after VSG, but RYGB directly bypasses the duodenum from nutritional influx, thereby restricting the intestinal absorption of fats and other nutrients (51, 52). While it is likely that different bariatric surgery strategies have different mechanistic impacts, decreased total nutrient intake is a fundamental common link. While VSG is thought to achieve this simply by decreased stomach capacity (53–55), our results suggest that the additional mechanism of decreased nutrient absorption may provide a shared mechanism underlying at least some of the metabolic effects of both RYGB and VSG.

Finally, the longer-term studies outlined here are associated with significant body weight changes and do not address mechanisms or pathways related to the well-recognized (56) but still unclear (57) acute metabolic benefits of bariatric surgery prior to substantial weight loss. However, the decreased caloric intake implied by the decreased lipid absorption in our studies is consistent with a recent human study showing that the metabolic benefits of bariatric surgery and simple weight loss due to decreased caloric intake are indistinguishable (58). Overall, we conclude that our results add decreased intestinal BAs and decreased lipid absorption as an unexpected but important additional contributor to the growing list of explanations for the metabolic benefits of bariatric surgery.

Materials and Methods

Generation of Genetic Mouse Models. Generation of global *Fxr*-null mice (*Fxr*$^{-/-}$) and homozygous *Fxr*-floxed mice (*Fxr*$^{fl/fl}$) was described previously (20). Briefly, the *Fxr*$^{-/-}$mice were generated by crossing the whole-body CRE line with *Fxr*-floxed mice to match the background of *Fxr*$^{\Delta L}$ and *Fxr*$^{\Delta IN}$ mice (20). To generate liver-specific *Fxr*-null mice (*Fxr*$^{\Delta L}$) and intestine-specific *Fxr*-null mice (*Fxr*$^{\Delta IN}$), homozygous *Fxr*-floxed mice (*Fxr*$^{fl/fl}$) were crossed with mice harboring the cre-recombinase under the control of the albumin promoter [Alb-Cre mice; Jackson Laboratory; stock no. 016832-B6.FVB(129)-Tg(Alb1-cre)1Dlr/J] and villin promoter [Villin-Cre mice; Jackson Laboratory; stock no. 004586-B6.Cg-Tg(Vil1-cre) 997Gum/J], respectively. *Cyp27a1* knockout mice (*Cyp27a1*$^{-/-}$) were from Jackson Laboratory (stock no. B6.129-Cyp27a1^{tm1Elt}/J). All colonies of mice were maintained on a C57BL/6 background.

Animals and Surgical Procedures. Animal experiments were approved by the Institutional Animal Care and Use Committees (IACUCs) of City of Hope,

Duarte (IACUC protocol: 14031). All the mice were maintained in a pathogen-free animal facility under standard 12:12-h light:dark cycle and housed in groups of three to five with unlimited access to water and standard rodent chow.

Male mice between 6 and 8 wk old were used in each group of experiments. Mouse cohorts received 60 kcal% saturated HFD (D12492; Research Diets) for 10 wk and were then randomly subdivided into two body weight-matched groups prior to surgery. VSG was performed in anesthetized mice (isoflurane) to remove ∼80% of the stomach as previously reported (19). Sham operation involved ligament dissection and pressure application on the stomach and was performed as previously described (18, 19). Following surgery, mice were housed in groups of two or three and fed with diet gel (DietGel Boost; Clear H_2O) for 3 d of the postoperative recovery period. Next, mice were maintained on HFD until they were euthanatized ∼4 or 12 wk after surgery, following a 4-h fasting (initiated at 6 AM). Body weight and food intake were measured by weighing the mice and their food hoppers weekly. For the BA supplementation study, TCA (Sigma; 0.2% wt/wt) was added to the HFD fed to $Fxr^{fl/fl}$-sham or $Fxr^{fl/fl}$-VSG mice for 6 wk and was initiated after postoperative recovery period.

Glucose Tolerance and Insulin Tolerance Tests. Fasting blood glucose levels were determined using a portable glucose meter (Abbot Laboratories), and fasting blood insulin levels were measured with the Mouse Insulin Elisa kit (Crystal Chem Inc.). For GTT, mice were fasted for 14 h and then injected intraperitoneally with D-glucose (1.5 g kg^{-1} body weight) that was dissolved in 0.9% saline; glucose levels were measured from tail blood before and 15, 30, 60, or 120 min postinjection, and areas under curve were calculated. For insulin tolerance test (ITT), mice were injected intraperitoneally with insulin (0.75 U kg^{-1} body weight) after they were fasted for 4 h; glucose levels were measured at the same time points as GTT.

Histological Analysis of Liver and Adipose Tissues. Paraffin sections and frozen sections were prepared by the Pathology Core Services of City of Hope National Medical Center. Paraffin sections were stained with hemotoxylin and eosin. Frozen sections were stained for neutral fat using an Oil red O staining and hematoxylin. Images were taken using the Olympus BX51TF microscope (Olympus Corporation).

Fecal Triglyceride Measurements. Feces were collected over a 24-h period at 4 wk post-VSG for the measurement of triglyceride levels. The collected fecal samples were dried and grinded into powder. Fifty milligrams of mixed feces was homogenized in 0.5 mL PBS; 0.4 mL of homogenate was added into 1.6 mL of $CHCl_3$-CH_3OH (chloroform/methanol, 2:1, vol/vol) mixture and mixed by vigorous shaking. The suspension was centrifuged at 3,000 rpm for 10 min at room temperature. The lower organic phase was transferred to a clean tube and air dried in a chemical hood overnight. After resuspending the residual liquid in 500 to 2,000 μL of 1% Triton X-100 in absolute ethanol, the concentration of triglyceride was determined using the commercial kits (Wako Life Sciences). Triglyceride level was normalized to 24-h fecal output.

BAs Profile Analysis. Mice were euthanatized, and samples of small intestine with luminal content were collected ∼4 wk after VSG surgery, following a 4-h fasting (initiated at 6 AM). BAs of the entire small intestine (with content) were extracted. Briefly, the entire small intestine with its luminal content from mice was homogenized in 7.5 mL of 75% ethanol. The homogenate was subsequently incubated at 50 °C for 2 h and centrifuged at 6,000 × *g* for 10 min at 4 °C. The supernatant fraction, which contained BAs, was collected. The total BA content was determined using a Total Bile Acids Colorimetric Assay kit (DIAZYME). BAs composition was analyzed using ultraperformance liquid chromatography–mass spectrometry as previously described (19).

Absorption of Dietary Fat. The surfactant tyloxapol (100 μL; 5% in PBS; Sigma) was injected into mice through a tail vein to inhibit the clearance of plasma triacylglycerol (28). After 15 min, mice were challenged with 200 μL of olive oil containing 2 μCi 14C-triolein. Blood was collected at baseline and time points 1, 2, 4, and 6 h. Fat absorption was determined by scintillation measurement (LS6500 Liquid Scintillation Counter; Beckman).

Distribution of Dietary Fat Uptake. The uptake of dietary fat along the length of the small intestine was assessed as described (28). Mice were fasted for 4 h and gavaged with 2 μCi ^{14}C-triolein in 200 μL of olive oil. Two hours later, the small intestine (between the base of the stomach and the cecal junction) was collected, flushed with 0.5 mM sodium taurocholate in PBS, and cut it into 3-cm segments. Segments were digested with 500 μL of 1 N NaOH at 65 °C for 1 h, mixed with 5 mL Liquid Scintillation Mixtures (ScintiSafe; Fisher Scientific), and measured (LS6500 Liquid Scintillation Counter; Beckman).

Lipid Staining of Proximal Jejunum. Mice were fasted for 4 h and gavaged with 200 μL olive oil. Two hours later, the proximal jejunum was collected and flushed with 0.5 mM sodium taurocholate in PBS. Sections were permeabilized with 0.2% Triton X-100 and incubated for 15 min with 4′,6-diamidino-2-phenylindole (DAPI) and BODIPY (10 μg mL^{-1}; Invitrogen) for nuclei and neutral lipid staining, respectively. Tissue sections were then washed three times with 1% bovine serum albumin (BSA)/phosphate-buffered saline (PBS) for 10 min. All samples were mounted in VECTASHIELD (Vector Laboratories) and covered with glass coverslips. Samples were examined under epifluorescent optics, and digital images were obtained with a scanning microscope (EVOS FL Auto; Thermo Scientific). The fluorescent signal intensity was determined by the average of three representative images from each mouse (n = 5 mice per group). Quantification of the mean fluorescence intensity was performed using the ImageJ software package.

RNA and Protein Analysis. Liver and ileum were collected at 4 wk postsurgery and subjected to total RNA extraction using TRIzol reagent (ZYMO Research). The first strand of complementary DNA (cDNA) was synthesized using all-In-One first Strand cDNA Synthesis Mix (Bioland). Real-time PCR (RT-PCR) was performed on ABI 7500 (Applied Biosystems) with SYBR Green quantitative PCR (qPCR) Supermix (Fisher Scientific). The primers for RT-PCR are available in *SI Appendix*, Table S1. Data were normalized against the housekeeping gene (36B4) and analyzed using the ΔΔcycle threshold (ΔΔCt) method. Protein, extracted from frozen livers using tissue lysis buffer (Pierce), was subjected to western blot analysis using antibodies against Bsep (arigo Biolaboratories Corp.; ARG10598) and glyceraldehyde 3-phosphate dehydrogenase (Gapdh) (Cell Signaling; #5174S) using standard methodology. Western blotting was performed as previously described (59). Quantification of the western blots was performed using the ImageJ software package, as described (59).

Microbiome Analysis. Mice on HFD for 4 wk after VSG and sham operation were euthanized by CO_2 asphyxiation. Cecal contents were collected immediately following asphyxiation. Microbiome genomic DNA was extracted using QIAamp DNA stool Mini Kit (Qiagen) according to the manufacturer's protocol. Sequencing library preparation, sequencing, and data analysis were performed by Integrative Genomics Core Facility at City of Hope National Medical Center as previously described (19).

Statistical Analysis. Experimental values are expressed as mean ± SEM. Statistical analyses were performed using the Student's t test (two tailed) or one-way ANOVA followed by Tukey's post hoc test. Statistical significance is displayed as follows: $^{*}P < 0.05$ or $^{**}P < 0.01$ vs. sham mice or $Fxr^{fl/fl}$-sham mice treated with TCA and $^{\#}P < 0.05$ or $^{\#\#}P < 0.01$ vs. VSG mice. All statistical analyses were performed using GraphPad Prism 6 (GraphPad Software).

Data Availability. All study data are included in the article and/or *SI Appendix*.

ACKNOWLEDGMENTS. We thank Dr. Art Riggs, Dr. Rama Natarajan, and Dr. Barry Forman for helpful discussions, along with Mr. William Davis and Mr. Allen Yeung for their support. We particularly thank Dr. Ian Talisman for editing the manuscript. This work is supported partially by National Natural Science Foundation of China Grants 81773961 (to L.D.), and 81920108033 (to Z.W.); Shanghai Pujiang Program Grant 17PJ1408800 (to L.D.); National Science and Technology (S&T) Major Special Projects of China Grant 2017ZX09309006 (to L.Y.); R.P. Doherty, Jr. Welch Professorship (Q-0022, D.D.M.) National Institute of Diabetes and Digestive and Kidney Diseases (NIDDK) Grant R01DK124627 (to W.H.); the Schaeffer Foundation (W.H.); and the Hench Foundation (W.H.).

1. G. Mingrone *et al*., Bariatric surgery versus conventional medical therapy for type 2 diabetes. *N. Engl. J. Med.* **366**, 1577–1585 (2012).
2. G. Mingrone *et al*., Bariatric-metabolic surgery versus conventional medical treatment in obese patients with type 2 diabetes: 5 Year follow-up of an open-label, single-centre, randomised controlled trial. *Lancet* **386**, 964–973 (2015).
3. L. Angrisani *et al*., Bariatric surgery worldwide 2013. *Obes. Surg.* **25**, 1822–1832 (2015).
4. J. P. Buwen, M. R. Kammerer, A. C. Beekley, D. S. Tichansky, Laparoscopic sleeve gastrectomy: The rightful gold standard weight loss surgery procedure. *Surg. Obes. Relat. Dis.* **11**, 1383–1385 (2015).

5. B. N. Reames, J. F. Finks, D. Bacal, A. M. Carlin, J. B. Dimick, Changes in bariatric surgery procedure use in Michigan, 2006-2013. *JAMA* **312**, 959–961 (2014).
6. M. A. Stefater, H. E. Wilson-Pérez, A. P. Chambers, D. A. Sandoval, R. J. Seeley, All bariatric surgeries are not created equal: Insights from mechanistic comparisons. *Endocr. Rev.* **33**, 595–622 (2012).
7. A. D. Miras, C. W. le Roux, Mechanisms underlying weight loss after bariatric surgery. *Nat. Rev. Gastroenterol. Hepatol.* **10**, 575–584 (2013).
8. A. P. Chambers *et al*., Regulation of gastric emptying rate and its role in nutrient-induced GLP-1 secretion in rats after vertical sleeve gastrectomy. *Am. J. Physiol. Endocrinol. Metab.* **306**, E424–E432 (2014).
9. R. E. Steinert *et al*., Bile acids and gut peptide secretion after bariatric surgery: A 1-year prospective randomized pilot trial. *Obesity (Silver Spring)* **21**, E660–E668 (2013).
10. J. D. Douros *et al*., Enhanced glucose control following vertical sleeve gastrectomy does not require a β-cell glucagon-like peptide 1 receptor. *Diabetes* **67**, 1504–1511 (2018).
11. J. D. Douros *et al*., Sleeve gastrectomy rapidly enhances islet function independently of body weight. *JCI Insight* **4**, e126688 (2019).
12. C. R. Flynn, V. L. Albaugh, N. N. Abumrad, Metabolic effects of bile acids: Potential role in bariatric surgery. *Cell. Mol. Gastroenterol. Hepatol.* **8**, 235–246 (2019).
13. H. Nakatani *et al*., Serum bile acid along with plasma incretins and serum high-molecular weight adiponectin levels are increased after bariatric surgery. *Metabolism* **58**, 1400–1407 (2009).
14. G. S. Gerhard *et al*., A role for fibroblast growth factor 19 and bile acids in diabetes remission after Roux-en-Y gastric bypass. *Diabetes Care* **36**, 1859–1864 (2013).
15. J. Tian *et al*., Bile acid signaling and bariatric surgery. *Liver Res.* **1**, 208–213 (2017).
16. A. Myronovych *et al*., Vertical sleeve gastrectomy reduces hepatic steatosis while increasing serum bile acids in a weight-loss-independent manner. *Obesity (Silver Spring)* **22**, 390–400 (2014).
17. A. Myronovych *et al*., The role of small heterodimer partner in nonalcoholic fatty liver disease improvement after sleeve gastrectomy in mice. *Obesity (Silver Spring)* **22**, 2301–2311 (2014).
18. K. K. Ryan *et al*., FXR is a molecular target for the effects of vertical sleeve gastrectomy. *Nature* **509**, 183–188 (2014).
19. L. Ding *et al*., Vertical sleeve gastrectomy activates GPBAR-1/TGR5 to sustain weight loss, improve fatty liver, and remit insulin resistance in mice. *Hepatology* **64**, 760–773 (2016).
20. L. Zhang *et al*., Promotion of liver regeneration/repair by farnesoid X receptor in both liver and intestine in mice. *Hepatology* **56**, 2336–2343 (2012).
21. S. Cipriani, A. Mencarelli, G. Palladino, S. Fiorucci, FXR activation reverses insulin resistance and lipid abnormalities and protects against liver steatosis in Zucker (fa/fa) obese rats. *J. Lipid Res.* **51**, 771–784 (2010).
22. S. Modica, S. Murzilli, L. Salvatore, D. R. Schmidt, A. Moschetta, Nuclear bile acid receptor FXR protects against intestinal tumorigenesis. *Cancer Res.* **68**, 9589–9594 (2008).
23. Y. Zhang *et al*., Activation of the nuclear receptor FXR improves hyperglycemia and hyperlipidemia in diabetic mice. *Proc. Natl. Acad. Sci. U.S.A.* **103**, 1006–1011 (2006).
24. A. R. Chopra *et al*., Cellular energy depletion resets whole-body energy by promoting coactivator-mediated dietary fuel absorption. *Cell Metab.* **13**, 35–43 (2011).
25. N. Gomez-Ospina *et al*., Mutations in the nuclear bile acid receptor FXR cause progressive familial intrahepatic cholestasis. *Nat. Commun.* **7**, 10713 (2016).
26. C. J. Sinal *et al*., Targeted disruption of the nuclear receptor FXR/BAR impairs bile acid and lipid homeostasis. *Cell* **102**, 731–744 (2000).
27. Y. Zhu, F. Li, G. L. Guo, Tissue-specific function of farnesoid X receptor in liver and intestine. *Pharmacol. Res.* **63**, 259–265 (2011).
28. C. L. Yen *et al*., Deficiency of the intestinal enzyme acyl CoA:monoacylglycerol acyltransferase-2 protects mice from metabolic disorders induced by high-fat feeding. *Nat. Med.* **15**, 442–446 (2009).
29. C. Murphy *et al*., Cholic acid as key regulator of cholesterol synthesis, intestinal absorption and hepatic storage in mice. *Biochim. Biophys. Acta* **1735**, 167–175 (2005).
30. R. A. Haeusler, B. Astiarraga, S. Camastra, D. Accili, E. Ferrannini, Human insulin resistance is associated with increased plasma levels of 12α-hydroxylated bile acids. *Diabetes* **62**, 4184–4191 (2013).
31. J. Y. Chiang, Bile acid metabolism and signaling. *Compr. Physiol.* **3**, 1191–1212 (2013).
32. J. M. Ridlon, S. C. Harris, S. Bhowmik, D. J. Kang, P. B. Hylemon, Consequences of bile salt biotransformations by intestinal bacteria. *Gut Microbes* **7**, 22–39 (2016).
33. D. Rizzolo *et al*., Bile acid homeostasis in a cholesterol 7α-hydroxylase and sterol 27-hydroxylase double knockout mouse model. *Hepatology* **70**, 389–402 (2019).
34. J. J. Repa *et al*., Disruption of the sterol 27-hydroxylase gene in mice results in hepatomegaly and hypertriglyceridemia. Reversal by cholic acid feeding. *J. Biol. Chem.* **275**, 39685–39692 (2000).
35. G. Lassailly *et al*, Bariatric surgery provides long-term resolution of nonalcoholic steatohepatitis and regression of fibrosis. *Gastroenterology* **159**, 1290–1301.e5 (2020).
36. M. Watanabe *et al*., Bile acids lower triglyceride levels via a pathway involving FXR, SHP, and SREBP-1c. *J. Clin. Invest.* **113**, 1408–1418 (2004).
37. K. Patel *et al*., Cilofexor, a nonsteroidal FXR agonist, in patients with noncirrhotic NASH: A phase 2 randomized controlled trial. *Hepatology* **72**, 58–71 (2020).
38. S. Fang *et al*., Intestinal FXR agonism promotes adipose tissue browning and reduces obesity and insulin resistance. *Nat. Med.* **21**, 159–165 (2015).
39. C. Jiang *et al*., Intestinal farnesoid X receptor signaling promotes nonalcoholic fatty liver disease. *J. Clin. Invest.* **125**, 386–402 (2015).
40. L. Sun *et al*., Gut microbiota and intestinal FXR mediate the clinical benefits of metformin. *Nat. Med.* **24**, 1919–1929 (2018).
41. F. J. Gonzalez, C. Jiang, A. D. Patterson, An intestinal microbiota-farnesoid X receptor axis modulates metabolic disease. *Gastroenterology* **151**, 845–859 (2016).
42. C. Jiang *et al*., Intestine-selective farnesoid X receptor inhibition improves obesity-related metabolic dysfunction. *Nat. Commun.* **6**, 10166 (2015).
43. V. L. Albaugh *et al*., Role of bile acids and GLP-1 in mediating the metabolic improvements of bariatric surgery. *Gastroenterology* **156**, 1041–1051.e4 (2019).
44. I. Kim *et al*., Differential regulation of bile acid homeostasis by the farnesoid X receptor in liver and intestine. *J. Lipid Res.* **48**, 2664–2672 (2007).
45. J. Y. Chiang, Regulation of bile acid synthesis. *Front. Biosci.* **3**, d176–d193 (1998).
46. C. Blanchard *et al*., Sleeve gastrectomy alters intestinal permeability in diet-induced obese mice. *Obes. Surg.* **27**, 2590–2598 (2017).
47. T. Inagaki *et al*., Regulation of antibacterial defense in the small intestine by the nuclear bile acid receptor. *Proc. Natl. Acad. Sci. U.S.A.* **103**, 3920–3925 (2006).
48. M. R. Jones, O. M. Nwose, Role of colesevelam in combination lipid-lowering therapy. *Am. J. Cardiovasc. Drugs* **13**, 315–323 (2013).
49. E. Zhou *et al*., Colesevelam enhances the beneficial effects of brown fat activation on hyperlipidaemia and atherosclerosis development. *Cardiovasc. Res.* 116, 1710–1720 (2020).
50. Y. Handelsman, Role of bile acid sequestrants in the treatment of type 2 diabetes. *Diabetes Care* 34 (suppl. 2), S244–S250 (2011).
51. R. Kumar *et al*., Fat malabsorption and increased intestinal oxalate absorption are common after Roux-en-Y gastric bypass surgery. *Surgery* 149, 654–661 (2011).
52. R. A. Sawaya, J. Jaffe, L. Friedenberg, F. K. Friedenberg, Vitamin, mineral, and drug absorption following bariatric surgery. *Curr. Drug Metab.* 13, 1345–1355 (2012).
53. A. A. Gumbs, M. Gagner, G. Dakin, A. Pomp, Sleeve gastrectomy for morbid obesity. *Obes. Surg.* 17, 962–969 (2007).
54. A. Baltasar *et al*., Laparoscopic sleeve gastrectomy: A multi-purpose bariatric operation. *Obes. Surg.* **15**, 1124–1128 (2005).
55. R. T. Yehoshua *et al*., Laparoscopic sleeve gastrectomy–Volume and pressure assessment. *Obes. Surg.* **18**, 1083–1088 (2008).Corrected in: *Obes. Surg.* **19**, 134 (2009).
56. J. D. Douros, J. Tong, D. A. D'Alessio, The effects of bariatric surgery on islet function, insulin secretion, and glucose control. *Endocr. Rev.* **40**, 1394–1423 (2019).
57. M. Chondronikola, L. L. S. Harris, S. Klein, Bariatric surgery and type 2 diabetes: Are there weight loss-independent therapeutic effects of upper gastrointestinal bypass? *J. Intern. Med.* **280**, 476–486 (2016).
58. M. Yoshino *et al*., Effects of diet versus gastric bypass on metabolic function in diabetes. *N. Engl. J. Med.* **383**, 721–732 (2020).
59. Y. Gu *et al*., CaMKII γ, a critical regulator of CML stem/progenitor cells, is a target of the natural product berbamine. *Blood* **120**, 4829–4839 (2012).